Driven Frenkel-Kontorova model. I. Uniform sliding states and dynamical domains of different particle densities

Torsten Strunz and Franz-Josef Elmer
Institut für Physik, Universität Basel, CH-4056 Basel, Switzerland
(Received 4 September 1997; revised manuscript received 5 February 1998)

The dynamical behavior of a harmonic chain in a spatially periodic potential (Frenkel-Kontorova model, discrete sine-Gordon equation) under the influence of an external force and a velocity proportional damping is investigated. We do this at zero temperature for long chains in a regime where inertia and damping as well as the nearest-neighbor interaction and the potential are of the same order. There are two types of regular sliding states: uniform sliding states, which are periodic solutions where all particles perform the same motion shifted in time; and nonuniform sliding states, which are quasiperiodic solutions where the system forms patterns of domains of different uniform sliding states. We discuss the properties of this kind of pattern formation, and derive equations of motion for the slowly varying average particle density and velocity. To observe these dynamical domains, we suggest experiments with a discrete ring of at least 50 Josephson junctions.
[S1063-651X(98)11608-2]

PACS number(s): 46.10.+z, 03.20.+i, 74.50.+r

I. INTRODUCTION

Sixty years ago, Frenkel and Kontorova introduced a simple model which has become popular in many fields of solid-state physics and nonlinear dynamics [1]. They invented their model in order to describe the motion of a dislocation in a crystal [2]. Meanwhile, the Frenkel-Kontorova (FK) model has become also a model for an adsorbate layer on the surface of a crystal [3,4], for ionic conductors [5,6], for glassy materials [5,4,7], for charge-density-wave (CDW) transport [8], for chains of coupled Josephson junctions [8,9], and for sliding friction [10].

The FK model is a chain of particles with mass m coupled by a harmonic nearest-neighbor interaction with stiffness κ. It is under the influence of an external spatially periodic potential with periodicity c and strength U_0. Here we study the nonequilibrium behavior of the FK model driven by a force $\tilde{F}$. We assume energy dissipation due to a usual damping force with a damping constant η. After rescaling time and space, one obtains the following equation of motion in dimensionless units:

$$\ddot{x}_j+\gamma\dot{x}_j=x_{j-1}+x_{j+1}-2x_j-b\,\sin x_j+F, \tag{1}$$

where $\gamma\equiv\eta/\sqrt{\kappa m}$, $b\equiv(2\pi/c)^2U_0/\kappa$, and $F\equiv(2\pi/c)\tilde{F}/\kappa$. The time and space units are $\sqrt{m/\kappa}$ and $c/2\pi$, respectively. We assume periodic boundary conditions, i.e.,

$$x_{j+N}=x_j+2\pi M, \tag{2}$$

where N is the number of particles and M is an arbitrary integer. Note that the periodic boundary condition implies that the average particle density $1/a$ is constant, i.e.,

$$a=2\pi\frac{M}{N}. \tag{3}$$

Due to symmetries, a can be restricted to $a\in[0,\pi]$ without loss of generality.

The dynamical behavior of the FK model has already been studied in several limits: (i) in the overdamped limit (i.e., $\ddot{x}_j$ can be neglected) for large N [8,11]; (ii) in the limit of zero damping and driving (i.e., $\gamma=F=0$) for $a/2\pi$ near integer values, allowing well separated 2π kinks [12] as well as for the most incommensurate value (i.e., the golden mean) of $a/2\pi$ [13]; and (iii) in the underdamped case for small N ($N\leqslant 10$) [9,14]. In a series of papers, Braun and coworkers recently studied recently the underdamped dynamics of a generalized FK model with $N>100$ but a near zero and π [15–17].

In this series of two papers, we study the underdamped FK model for large numbers of particles (i.e., $N>100$). We do not restrict ourselves to values of $a/2\pi$ near integer or half integer values where the dynamical behavior can be described in terms of kinks. The system has stationary, periodic, quasiperiodic, and chaotic solutions. Of special interest is the transition from stationarity to sliding, the so-called *pinning-depinning transition*, and the backward process. In the first paper, we investigate the periodic and quasiperiodic solutions. The second paper will be concerned with the depinning-pinning transition between stationary states and spatiotemporal chaos. Preliminary results have already been published in a conference proceedings [18].

In Sec. IV, we will see that the FK model spontaneously forms spatial-temporal patterns as many other spatially extended systems driven far from equilibrium [19]. These patterns are caused by the bistability and instability of the *uniform sliding state*. In the uniform sliding state all particles perform exactly the same regular and periodic motion. Different particles differ only in the phase of this motion. The phase difference of two neighboring particles is the same

everywhere. That is, the density of particles is on average constant along the chain. The uniform sliding state is the only nonstationary state in the overdamped limit [20] but it has also be studied in the underdamped case [9,21].

The discreteness of the chain leads to several *resonances* in the underdamped limit [9,14,21,22]. The consequence is bistability. For spatially extended bistable systems it is well known that domainlike patterns are possible [19]. In the FK model these domains can be characterized by the average particle density $1/a$ and the average particle velocity v. We find that states with two or three different types of domains survive in the long-time limit. The number and the width of the domains can vary, leading to a quite large number of possible solutions. Because of different average velocities in different domain types, the motion in the domain solutions is quasiperiodic. Assuming that a and v are slowly varying functions in time and space, we derive an approximate equation of motion for them. With its help we understand why the domains do not disappear in the long-time limit, and why there are not more than three different domain types. Furthermore, it turns out that the state in the long-time limit can be understood as a spatially chaotic solution of a corresponding dynamical system. A special variant of these domain solutions is the *traffic-jam state* where the particle velocity in one domain is zero [15–17].

The paper is organized as follows: In Sec. II, we derive two different but mathematically equivalent formulas for the relation between the force F and the average sliding velocity v. In Sec. III, the periodic solution (i.e., the uniform sliding state) and its stability are discussed. The domainlike states are investigated in Sec. IV. In Sec. V, the main part of the paper concludes with some remarks concerning possible experimental observations of these domainlike states and similarities to other pattern forming systems. The appendixes describe our numerical and analytical scheme to obtain the uniform sliding state and to analyze its stability.

II. AVERAGE SLIDING VELOCITY AND EFFECTIVE FRICTION FORCE

The *average sliding velocity* v of the chain reads

$$v=\lim_{T\to\infty}\frac{1}{T}\int_0^T\frac{1}{N}\sum_{j=1}^{N}\dot{x}_j dt. \tag{4}$$

Plotting the measured or calculated values of v for different values of the applied force F, one obtains the so-called *velocity-force characteristic*. In CDW systems and Josephson-junction arrays, it corresponds to the current-voltage and voltage-current characteristics, respectively. In the context of friction, F can be interpreted as the effective kinetic friction as a function of the sliding velocity v.

There are two mathematically equivalent relationships between F and v. The first one can be obtained by taking the time average of the sum of Eq. (1) over all particles:

$$F=\gamma v+\lim_{T\to\infty}\frac{1}{T}\int_0^T\frac{b}{N}\sum_{j=1}^{N}\sin x_j(t)dt. \tag{5}$$

This formula assumes that the average acceleration of the chain is zero. The other relationship can be derived from the fact that the energy released during sliding has to be dissipated totally, i.e.,

$$Fv=\gamma\lim_{T\to\infty}\frac{1}{T}\int_0^T\frac{1}{N}\sum_{j=1}^{N}\dot{x}_j^2 dt.$$

Using Eq. (4), we obtain

$$F=\gamma v\left[1+\lim_{T\to\infty}\frac{1}{T}\int_0^T\frac{1}{N}\sum_{j=1}^{N}\left(\frac{\dot{x}_j}{v}-1\right)^2 dt\right]. \tag{6}$$

This result clearly shows that in the case of no dissipation (i.e., $\gamma=0$) the chain may slide without any applied force. In Sec. III B, we will discuss the condition of this possibility. Equation (6) also shows that the mobility v/F is always less than or equal to $1/\gamma$, i.e., the mobility in the limit $b\to 0$.

III. UNIFORM SLIDING

Because of the symmetries of the equation of motion, there exist nonstationary solutions called *uniform sliding states*. They are characterized by the fact that every particle performs the same motion but is shifted in time. That is, $x_{j+1}(t)=x_j(t+T_1)$, for $j=1,\ldots,N$. Thus we need only one function, the *dynamic hull function* f, to describe the motion of all particles [21,11,8,9]:

$$x_j(t)=\psi+aj+vt+f(\psi+aj+vt), \tag{7}$$

where v is the average sliding velocity and ψ is an arbitrary phase. Because of the discrete translation symmetry of Eq. (1), the Hull function is periodic, i.e.,

$$f(\varphi+2\pi)=f(\varphi). \tag{8}$$

Plugging ansatz (7) into the equation motion (1) leads to a differential delay equation for the hull function $f(\varphi)$:

$$v^2 f''(\varphi)+\gamma v[1+f'(\varphi)]=f(\varphi+a)+f(\varphi-a)-2f(\varphi)-b\,\sin[\varphi+f(\varphi)]+F. \tag{9}$$

The average sliding velocity v has to be chosen in such a way that a 2π-periodic function fulfills Eq. (9). If $f(\varphi)$ is a solution, then $f(\varphi+\psi)+\psi$ is also a solution. We make the definition of the dynamic hull function unique by restricting the solutions of Eq. (9) to 2π-periodic functions with zero average, i.e.,

$$\int_0^{2\pi} f(\varphi)d\varphi=0. \tag{10}$$

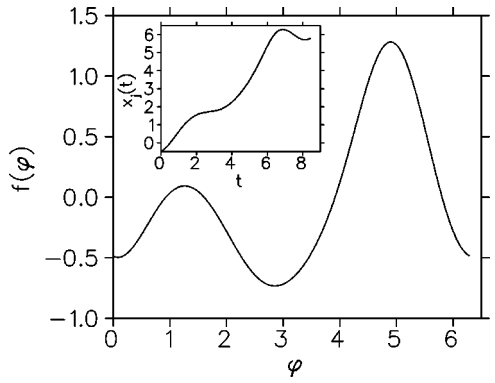

FIG. 1. The dynamic hull function $f(\varphi)$. The inset shows the corresponding particle position as a function of time. The parameters are $a/2\pi=(3-\sqrt{5})/2$, $b=2$, $v=0.75$, and $\gamma=0.5$. Because the solution is obtained by the method described in Appendix A, the average sliding velocity v is prescribed. The corresponding value of F is approximately 0.74.

For the uniform sliding state (9), the relationships (5) and (6) between v and F reduce to

$$F=\gamma v+\frac{b}{2\pi}\int_0^{2\pi}\sin[\varphi+f(\varphi)]d\varphi \tag{11}$$

and

$$F=\gamma v\left(1+\frac{1}{2\pi}\int_0^{2\pi}[f'(\varphi)]^2 d\varphi\right), \tag{12}$$

respectively.

Instead of solving Eq. (9) for a given value of F, it is more convenient to replace F by Eq. (11) or (12) and solve Eq. (9) for a given value of v. From the solution $f(\varphi)$ one obtains the corresponding F. In the overdamped limit, it is well known that F is a monotonically increasing function of v [20,8]. In the underdamped case, *resonances* lead to nonmonotonic velocity-force characteristics [23].

A. Resonances

We solve the hull-function equation (9) numerically by expanding f into a Fourier series. The details are described in Appendix A. Figure 1 shows an example of a dynamic Hull function.

In the underdamped case the numerically obtained velocity-force characteristics exhibits clearly peaks, as can be seen in Fig. 2. Near these peaks an increase of the driving force F by a considerable amount leads only to a slight increase of the average velocity v. In other words, the differential mobility dv/dF is much lower than the mobility without any periodic potential (i.e., $1/\gamma$). The reason for this behavior is that the additional energy is only partially turned into a larger kinetic energy of the center of mass of the chain, whereas the main part is turned into oscillatory motion of the particle due to resonances.

In the frame of the center of mass which moves with average sliding velocity v, the external potential leads to a time-periodic force acting on the particle. The frequency of this force, the so-called ''washboard frequency,'' is given by

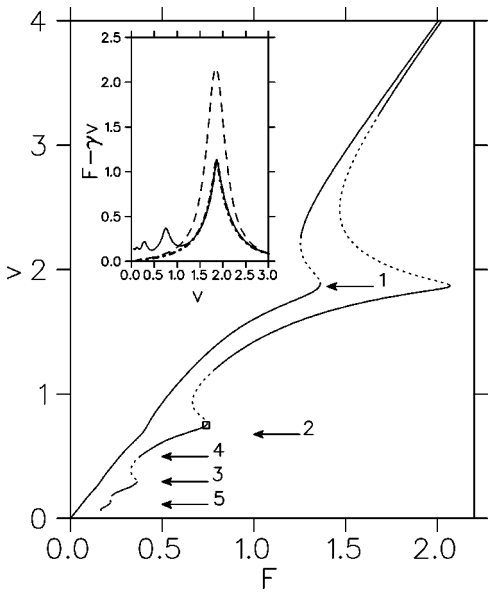

FIG. 2. Velocity-force characteristic of the uniform sliding state (7). Solid (dotted) lines indicate stable (unstable) solutions. Dashed and dashed-dotted lines in the inset denote analytically obtained approximations given by Eqs. (15) and (A9), respectively. The parameters are $a/2\pi=(3-\sqrt{5})/2$, $\gamma=0.5$, and $b=1$ (left curve) and $b=2$ (right curve and inset). The arrows denote the resonant values of v given by Eq. (16). The numbers indicate the order n.

the velocity of the center of mass divided by the period of the potential. Resonance occurs if the washboard frequency is equal to the eigenfrequency of the phonon with wave number $k=a$. To see this, we solve Eq. (9) in the approximation $\sin[\varphi+f(\varphi)]\approx\sin\varphi$. We obtain

$$f(\varphi)\approx\frac{ib/2}{\omega^2(a)-v^2+i\gamma v}e^{i\varphi}+\text{c.c.}, \tag{13}$$

where $\omega(k)$ is the phonon dispersion relation

$$\omega(k)=2\left|\sin\left(\frac{k}{2}\right)\right|. \tag{14}$$

In order to obtain the corresponding value of F, one can use either Eq. (11) or Eq. (12). Although both equations are equivalent, for the approximation (13) we obtain different results. Evaluating Eq. (11) leads to the obviously wrong result $F=\gamma v$. This can be understood from the fact that Eq. (13) is only the leading term of an expansion of the hull function in powers of b. Thus $F=\gamma v+O(b^2)$. Instead of calculating the next order in f, one can use Eq. (12), which leads to

$$F=\gamma v\left(1+\frac{b^2/2}{[\omega^2(a)-v^2]^2+\gamma^2 v^2}+O(b^4)\right). \tag{15}$$

Note that F has to be an even function of b because the external potential $b\cos x$ is an odd function of $x-\pi/2$. For large values of v, Eq. (13) approaches zero, and therefore $F\to\gamma v$. That is, if the washboard slides very fast, the par-

ticles cannot follow the swift pushing by the washboard. Thus the chain slides like a rigid solid. We call this state the *solid-sliding state*.

Figure 2 shows that for large values of b (or small values of γ) the simple approximation (15) overestimates the strength of the resonance line. That is, there is an effective damping, larger than γ, which increases with increasing oscillation amplitude. This larger damping can be understood by phonon coupling due to the nonlinearity in the equation of motion. This coupling opens up additional channels for energy dissipation yielding a higher effective damping constant. The inset of Fig. 2 shows that a remarkably good approximation of these additional dissipation processes is given by the Galerkin approximation $f(\varphi)=A\cos(\varphi+\psi)$. Projecting the hull-function equation (9) together with this ansatz onto $\sin\varphi$ and $\cos\varphi$ leads to two transcendental equations for A and ψ. After elimination of ψ, one can parametrize the velocity-force characteristic by the amplitude A [see Eq. (A9) in Appendix A].

In order to understand the other resonance peaks seen in Fig. 2, one has to keep in mind that the external potential not only leads to a periodic driving force, but also to a modulation of the eigenfrequencies. Thus parametric processes make it possible to excite other phonons. In the framework of a perturbation theory with b as the smallness parameter, the elementary processes corresponding to these resonance lines are the decay of n ''washboard waves'' (wave number a, frequency v) into a single phonon with wave number k and frequency $\omega(k)$. Assuming momentum and energy conservation, one obtains $k=na$ and $v=v_n$, where v_n is the *superharmonic resonance* frequency of order n:

$$v_n \equiv \frac{\omega(na)}{n}. \tag{16}$$

The positions of the first few resonances are shown in Fig. 2. The agreement with the actual positions of the resonance peaks is quite good. Near the superharmonic resonance of order n, the nth Fourier mode of the hull function has a maximum. For example, the square in Fig. 2 corresponds to the hull function in Fig. 1, which is clearly dominated by $\exp(2i\varphi)$. Because of finite dissipation, superharmonic resonances of higher order may be hidden behind a nearby resonance of lesser order such as, e.g., the fourth resonance in Fig. 2.

The superharmonic resonance has been already investigated in the literature, experimentally [24] as well as theoretically [12,14,21,22]. The superharmonic resonance condition (16) was observed first in numerical experiments by Aubry and de Seze [21,22]. They studied the FK model without damping but with a very small driving force. They found that the velocity of the center of mass did not increase linearly in time but it was locked for finite time intervals at velocities given by Eq. (16). They also studied the underdamped and driven FK model [21]. Peyrard and Kruskal found the same locking phenomenon for the velocity of a 2π kink [12]. In this case the resonance frequencies are given by

$$\tilde{v}_n \equiv \frac{\tilde{\omega}(na)}{n} \quad \text{with} \quad \tilde{\omega}(k)=\sqrt{b+\omega^2(k)}. \tag{17}$$

Ustinov, Cirillo, and Malomed also observed resonance lines in numerical simulations of the damped and driven FK model [14]. Van der Zant *et al.* reported evidence of these resonances in experiments with a ring of eight Josephson junctions [24].

The authors of Refs. [14] and [24] explained the resonances found by the following mechanism, which leads to Eq. (17). The mechanism relies on the assumption that 2π kinks travel in the ring. Most of the time the particles are in a potential well. When a kink travels through a particle, it jumps into the neighboring well and oscillates. Because of the periodic boundary conditions the jumps occur in equidistant time steps. The distance between two kinks in terms of the number of particles in between is given by $N/M=2\pi/a$. The kink velocity c is related to the average sliding velocity v by $v=ac$. Superharmonic resonances of order n occur if the time interval between two jumps, i.e., $(N/M)/c=2\pi/v$, is n times the oscillation time of the particles, i.e., $2\pi n/\tilde{\omega}(k)$, where $\tilde{\gamma}(k)$ given by Eq. (17), is the dispersion relation of the linearized equation of motion (1). The wave number k times the distance N/M has to be $2\pi n$, that is, $k=an$. According to this mechanism the superharmonic resonance condition is therefore Eq. (17). This picture is valid only if the distance between two kinks, i.e., $N/M=2\pi/a$, is much larger than 1. That is, the motion can be described by kinks only if $a/2\pi$ is near an integer value. Thus we expect that Eq. (16) is valid for $a=O(1)$, and Eq. (17) for $a\ll 1$. For example, the numerically obtained values of positions of the resonance peaks reported by Watanabe *et al.* [9] are closer to Eq. (16) than to Eq. (17) because $a>1$.

B. Instabilities

In order to discuss the instability of the uniform sliding state (7), one has to investigate the dynamics of small perturbations δx_j. They are governed by the equation of motion (1) linearized around Eq. (7):

$$\delta\ddot{x}_j+\gamma\delta\dot{x}_j=\delta x_{j-1}+\delta x_{j+1}-2\delta x_j - b\cos[aj+vt+f(aj+vt)]\delta x_j. \tag{18}$$

The periodic boundary condition (2) turns into $\delta x_{j+N}=\delta x_j$. In accordance with the Floquet-Bloch theorem, one can write any solution of this equation as a sum of solutions of the form

$$\delta x_j(t)=c_k(aj+vt)e^{(2\pi i/N)kj+\lambda_k t}, \quad k=1,\ldots,N, \tag{19}$$

where $c_k(\varphi)$ is a 2π periodic function, and λ_k is the so-called Floquet exponent. The uniform sliding state is stable if the real part of λ_k is negative for all values of k. There is always a solution with $\lambda_0=0$. It is the Goldstone mode $\delta x_j=\partial_t x_j=v+vf'(aj+vt)\equiv c_0(aj+vt)$, which follows directly from differentiating Eq. (9). Appendix B describes the scheme we used to solve Eq. (18) numerically with the Floquet-Bloch ansatz (19). The dotted lines in Fig. 2 denote unstable parts of the velocity-force characteristics.

Two different mechanisms may lead to an instability of the uniform sliding state. The first one is *negative differential mobility*, i.e., a negative slope in the velocity-force charac-

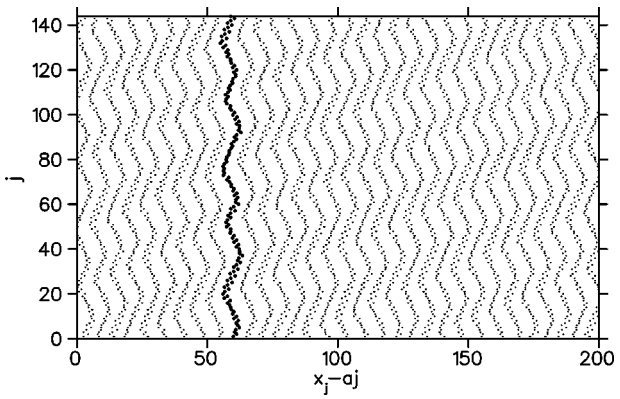

FIG. 3. Dynamical domains of different particle densities. A series of snapshots taken at equidistant time steps ($\delta t = 2\pi/v$) are shown. Each dot denotes the position of a particle. A particular zigzag shaped snapshot is highlighted. The zigs and zags correspond to two different kinds of domains that are characterized by uniform sliding. The parameters are $N=144$, $M=55$, $b=2$, $\gamma=0.5$, and $F=0.8$.

teristic. A small positive velocity fluctuation $v \to v+\delta v$ accelerates the chain because the applied force is larger than the force necessary to keep the new velocity $v+\delta v$ constant.

The second type of instabilities is caused by *parametric resonance*. In the framework of the multiphonon process, it corresponds to the decay of n washboard waves into two phonons with wave number $na/2 \pm q$. A parametric resonance of order n can be expected for values of the average sliding velocity v, which are given by

$$v_n^P(q) = \frac{\omega(na/2+q)+\omega(na/2-q)}{n}. \tag{20}$$

Because parametric resonance is a threshold phenomenon, the amplitude b of the washboard wave has to exceed a critical value which is proportional to $\gamma^{1/n}$ [19,25]. This is true only for values of v between the minimum and maximum of Eq. (20). For velocities outside this interval parametric resonance is still possible, but the threshold increases. For zero damping the uniform sliding state is unstable for any value of v below a certain critical value v_c, which is approximately calculated in Appendix B:

$$v_c \approx \sqrt{16\cos^2\left(\frac{a}{4}\right)+2b}. \tag{21}$$

The actual value of v_c obtained from the numerical stability analysis agrees very well with this formula even for large values of b. The numerical value of v_c is less than Eq. (21), but deviates not more than 10% for $b<4$.

IV. SLIDING DOMAINS

Near resonance peaks, the system is bistable and has therefore the opportunity to organize itself into *domains* of different uniform sliding states. Figure 3 shows a typical example with ten domains. There are only two types of domains. Each domain is characterized by uniform sliding. That is, in each domain the particle motion is given by Eq. (7), but the Hull function f and the value of a and v are different in each domain. One can say that the domains are characterized by different particle densities $1/a$. Neighboring domains are separated by domain walls (fronts) of finite size. Conservation of the number of particles implies that a front has to move with a velocity

$$v_{\text{front}} = \frac{a_2 v_1 - a_1 v_2}{a_2 - a_1}, \tag{22}$$

where the average particle distance and the average particle velocity of each domain type is given by $a_{1,2}$ and $v_{1,2}$, respectively. From the viewpoint of the particles, we can express the front velocity in terms of how fast the front travels from one particle to the next. It is given by

$$c = \frac{v_1 - v_2}{a_2 - a_1}. \tag{23}$$

Because Eqs. (22) and (23) are symmetric in the exchange of the indices, all fronts propagate with the same velocity, leaving the widths of the domains constant. The numbers $N_{1,2}$ of particles in each type of domain fulfill the constraints

$$N_1 + N_2 = N \quad \text{and} \quad a_1 N_1 + a_2 N_2 = 2\pi M = aN. \tag{24}$$

Because of $0 < N_{1,2} < N$, the particle density for one type of the domains is larger than $1/a$, whereas for the other type it is less than $1/a$. In the following the type with the larger density will be number 1. Thus

$$a_1 < a < a_2. \tag{25}$$

The average sliding velocity v of a domain state is given by

$$v = \frac{v_1 N_1 + v_2 N_2}{N}. \tag{26}$$

A domain-type state is in general a quasiperiodic motion with three frequencies: v_1 and v_2 from the periodic motion in each domain type; and $2\pi c/N$ from the cyclic motion of the fronts through the system.

A. Two-domain state

To understand this kind of pattern formation we investigate two-domain states in detail. First, we have to discuss the relationship between the average sliding velocity v and the average particle distance a for the uniform sliding state at a fixed value of F, i.e., the *velocity-distance characteristic*. A typical example is shown in Fig. 4(a). As in the velocity-force characteristic, resonances are responsible for folds.

A two-domain state is completely characterized by two points on the stable branches of the velocity-distance characteristic which fulfill Eq. (25). The velocity c of the front is the slope of the line connecting both points (see Fig. 7). The sizes of the domains are determined by the solutions of Eq. (24).

From this consideration, one would expect a continuous family of two-domain states parametrized by two real numbers. But this is not the case, as Fig. 5 clearly shows. In our numerical simulations we always found that the system dynamically selects the same pair of points on the velocity-distance characteristic. This is true even if a is changed as

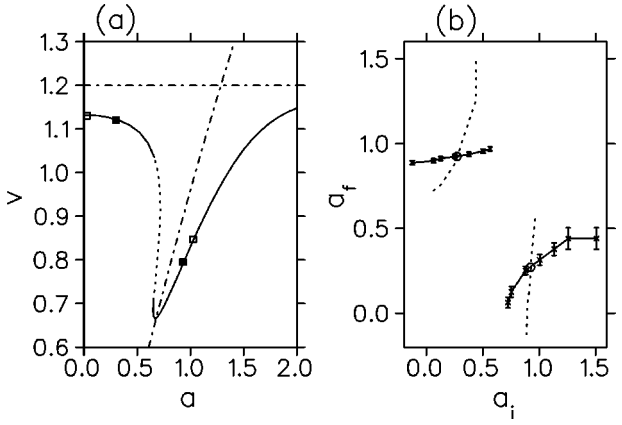

FIG. 4. (a) The velocity-distance characteristic for the uniform sliding states. Solid (dotted) lines indicate stable (unstable) states. The dash-dotted horizontal (tilted) line denotes $v=F/\gamma$ (the main resonance v_1). The open (filled) squares denote the initial (final) domain states of the simulation shown in Fig. 5. (b) The numerically obtained values of the average particle distances a_f behind the front for a given value a_i in front of the front. Those data points are connected by a solid line where a continuous function is expected. The dotted line denotes the inverse function. The circle near the intersection of both functions denotes the values of a_1 and a_2 of the numerically found two-domain solution. The parameters are $b=0.5$, $\gamma=0.5$, and $F=0.6$.

long as $a\in(a_1,a_2)$. How does the system select a certain pair of values for $a_{1,2}$? A careful inspection of Fig. 5 reveals that behind the fronts new domain states are selected. These states are independent of the initial states. The interface between the new domain state and the old one does not form a front. It smears out, and in the long-time limit the domain states approach to uniform densities with well-defined values of a. Numerical experiments show that the state a_f behind the front is uniquely defined by the state a_i in front of the front [see Fig. 4(b)]. Hence there is functional relation between them:

$$a_f=A(a_i). \tag{27}$$

Together with Eq. (23), we have a uniquely defined relation

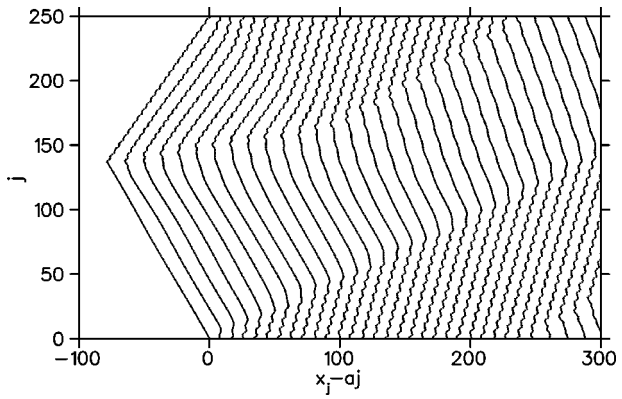

FIG. 5. Snapshots of the evolution of a two-domain state taken at equidistant time steps ($\Delta t=12$). The presentation is the same as in Fig. 3. The initial state is a two-domain state with $a_1=2\pi/100$ and $a_2=2\pi/5$. The initial positions and velocities of the particles are calculated by using Eq. (7). The parameters are $N=250$, $M=25$, $b=0.5$, $\gamma=0.5$, and $F=0.6$.

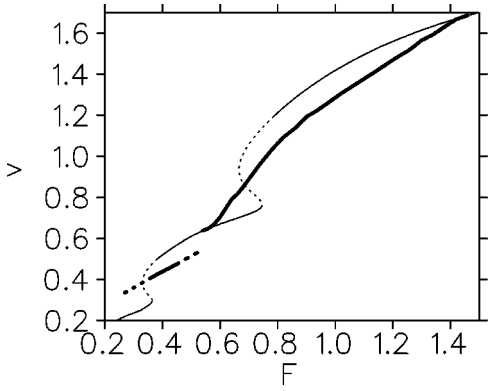

FIG. 6. Velocity-force characteristics for the uniform sliding states and the two-domain states. Thick (thin) lines denote two-domain (uniform sliding) states. Solid (dotted) lines indicate stable (unstable) solutions. The parameters are $N=2584$, $M=987$, $b=2$, and $\gamma=0.5$.

between c, a_i, and a_f. This behavior fits into the general picture of front propagation in bistable systems [19] (see also Sec. IV B). If we know function A, we can calculate the values of a_1 and a_2 by solving $A^{-1}(a)=A(a)$ [see also Fig. 4(b)]. Note that the values of a_1 and a_2 are in general irrational [26]. The value of a determines only the sizes of the domains. Whether the chain is commensurate or incommensurate is irrelevant. But numerically we have never found such states for values of a near integer multiples of 2π.

The selected values of a_1 and a_2 are of course functions of the applied force F. Figure 6 shows the velocity-force characteristic of the two-domain states. By varying F they disappear due to two reasons. First, one of the domains shrinks to zero, and the velocity-force characteristics of the two-domain state and uniform sliding state come together. Second, a_1 or a_2 may move onto an unstable branch of the velocity-distance characteristic. Thus the two-domain state still exists but it has become unstable. In Fig. 6, the velocity-force characteristic of this unstable two-domain state is denoted schematically by dotted extensions.

B. Quasicontinuum description of the front

We have seen that the state of the domains can be described by Eq. (7). They are characterized by $a_{1,2}$ and $v_{1,2}$. To describe the fronts in the same way, we assume that a and v are continuous functions which are varying slowly in space and time. The space coordinate is the particle index j. It becomes a real variable in a quasicontinuum description. Thus we write $x_j(t)=x(j,t)$. The discrete Laplacian $x_{j+1}+x_{j-1}-2x_j$ can be written as an infinite series of differential operators, i.e.,

$$x_{j+1}(t)+x_{j-1}(t)-2x_j(t)=4\,\sinh^2\left(\frac{1}{2}\partial_j\right)x(j,t). \tag{28}$$

We generalize the ansatz (7) by assuming that φ is a function of j and t, i.e.,

$$x(j,t)=\varphi(j,t)+f(\varphi(j,t)),\quad f(\varphi+2\pi)=f(\varphi), \tag{29}$$

where f is the solution of the Hull function equation (9). Now we define local values of a and v by

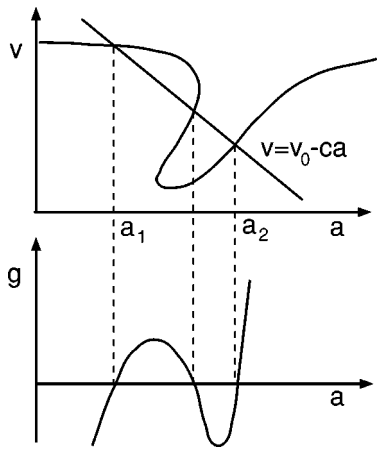

FIG. 7. Schematical drawing of the velocity-distance characteristic and the corresponding nonlinearity g.

$$a \equiv \partial_j \varphi, \quad \text{and} \quad v \equiv \partial_t \varphi. \tag{30}$$

Plugging the ansatz (29) into the equation of motion (1) and averaging over the phase φ, we obtain

$$\partial_t v = D(\partial_j)\partial_j a + F - F_U(a,v), \tag{31a}$$

$$\partial_t a = \partial_j v, \tag{31b}$$

where

$$D(x) \equiv \left(\frac{\sinh x/2}{x/2}\right)^2 = 1 + \frac{x^2}{12} + O(x^4), \tag{31c}$$

and $F_U(a,v)$ is the velocity-force characteristic of the uniform sliding state given by Eq. (11). Equation (31a) is only approximately correct because we have assumed that the Hull function f does not depend on a and v. Furthermore, the ansatz (29) cannot be exact in a front. Nevertheless, the approximation (31) is correct in leading order of a multiple-scale perturbation theory [27,28].

In general, Eq. (31) cannot be solved analytically. But we are able to discuss the front solutions qualitatively. Assuming stationarity of the front in the comoving frame, we obtain

$$a(j,t) = a(j-ct), \quad v(j,t) = v(j-ct), \tag{32}$$

where c is the front velocity (23). From Eq. (31b), we obtain $-ca' = v'$, which can be integrated leading to

$$v = v_0 - ca. \tag{33}$$

Plugging Eqs. (32) and (33) into Eq. (31a), and keeping only the first two terms of D, yields

$$(1-c^2)a' + \tfrac{1}{12}a''' + g(a,v_0,c) = 0, \tag{34}$$

with

$$g(a,v_0,c) \equiv F - F_U(a, v_0 - ca). \tag{35}$$

Equation (33) means a straight line in the velocity-distance characteristics (see Fig. 7). Front solutions exist for those values of v_0 and c for which Eq. (33) intersects the velocity-distance characteristic of the uniform sliding state three times. The two outside intersection points have to lead to stable uniform sliding states (characterized by a_1 and a_2), whereas the inner point has to belong to an unstable uniform sliding state. This is the reason why two-domain and multi-domain solutions appear only near resonance points where the velocity-force characteristic has a negative slope (see Fig. 6). Because there is no resonance for $a/2\pi$ integer, we understand why we have not found two-domain solutions for values of a close to integer multiples of 2π.

If the requirements on v_0 and c are fulfilled, the nonlinear term g in Eq. (34) will have three nodes and will be N shaped (see Fig. 7). A front solution is a heteroclinic orbit of Eq. (34), which goes from a_1 to a_2 or vice versa. Thus we are looking for solutions with boundary conditions $a(-\infty) = a_{1,2}$ and $a(\infty) = a_{2,1}$. A heteroclinic orbit occurs only if the unstable manifold of the fixed point $a_{1,2}$ is the stable manifold of $a_{2,1}$. This is possible only on a one-dimensional manifold in the parameter space of v_0 and c. Thus Eq. (27) is justified.

To calculate the stable and unstable manifolds, we linearize Eq. (34) around the fixed points $a_{1,2}$. For the perturbation $\delta a \equiv a - a_{1,2}$ we make the ansatz $\delta a = \exp(\lambda j)$, which leads to the characteristic polynomial

$$\tfrac{1}{12}\lambda^3 + (1-c^2)\lambda + \partial_a g(a_{1,2}) = 0. \tag{36}$$

Because of $\partial_a g(a_{1,2}) > 0$ (see Fig. 7), there is one negative root $\lambda_1 < 0$. If $(1-c^2)^3 + (3\partial_a g/4)^2 > 0$, the two other solutions are conjugated complex with a real part that is just $-\lambda_1/2$. Numerically we always found subsonic front motion (i.e., $|c| < 1$), leading to an unstable manifold that spirals out of the fixed point. Thus the precursor of the front is nonoscillatory, whereas its tail is oscillatory because the particles have inertia and therefore respond with an exponentially decreasing oscillation after an acceleration or deacceleration.

In order to verify this qualitative picture numerically, one has to extract a and v from the data. In principle this could be done by local fits of the dynamic Hull function, from which we obtain $\varphi(j,t)$ and subsequently a and v. But this is a very tedious way which is not necessary because we are only interested in the qualitative form of the shape of the front. The following simple method is sufficient for this task. For uniform sliding states, this leads to values of a and v which are identical to the exact ones. For each particle we introduce a sequence of times $t_{n,j}$ defined by $x_j(t_{n,j}) = (2n+1)\pi$ and $\dot{x}_j(t_{n,j}) > 0$. From these sequences, we obtain the following approximations for v and a:

$$v(j,t) \approx \frac{2\pi}{t_{n,j} - t_{n-1,j}}, \quad a(j,t) \approx v(j,t)(t_{m,j-1} - t_{n,j}), \tag{37}$$

where n and m are chosen in such a way that (i) $t_{n-1,j} < t < t_{n,j}$, and (ii) $t_{m,j-1}$ is the time closest to $t_{n,j}$, i.e., $|t_{m,j-1} - t_{n,j}| = \min_{\tilde{n}} |t_{\tilde{n},j-1} - t_{n,j}|$. This definition of a is necessary in order to avoid spurious values which differ from the expected value by $\pm 2\pi$.

For a fixed value of t, one obtains a snapshot of v and a. The superposition of many snapshots shifted by ct gives the impression of a smooth curve (see Fig. 8). We have tuned c until the curves are as smooth as possible. It turned out that

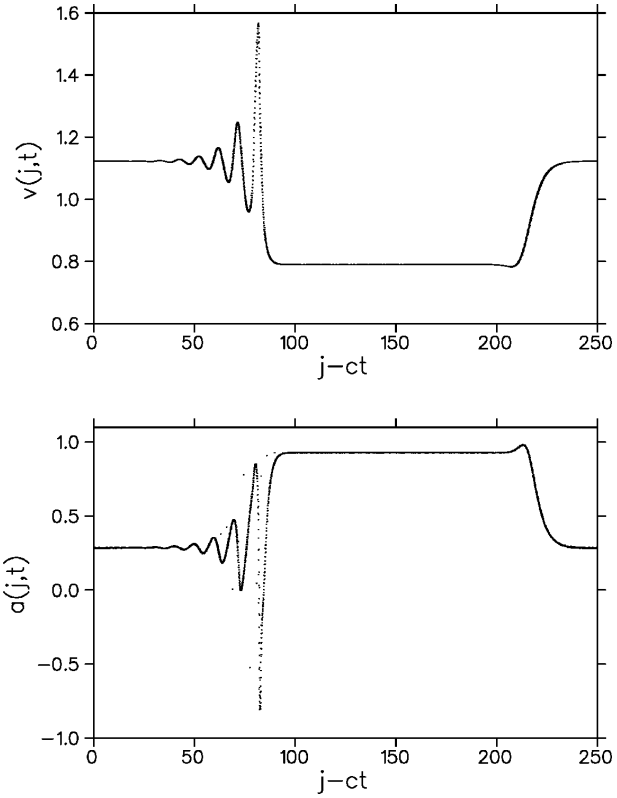

FIG. 8. Quasicontinuum description of the two-domain solution. The values of v and a are obtained from formulas (37). 20 snapshots taken at different times and shifted by ct are superimposed in order to obtain the details of the fronts. The value of c is chosen in such a way that the superimposition yields a smooth curve. The best value of c is 0.516. The parameters are the same as in Fig. 5.

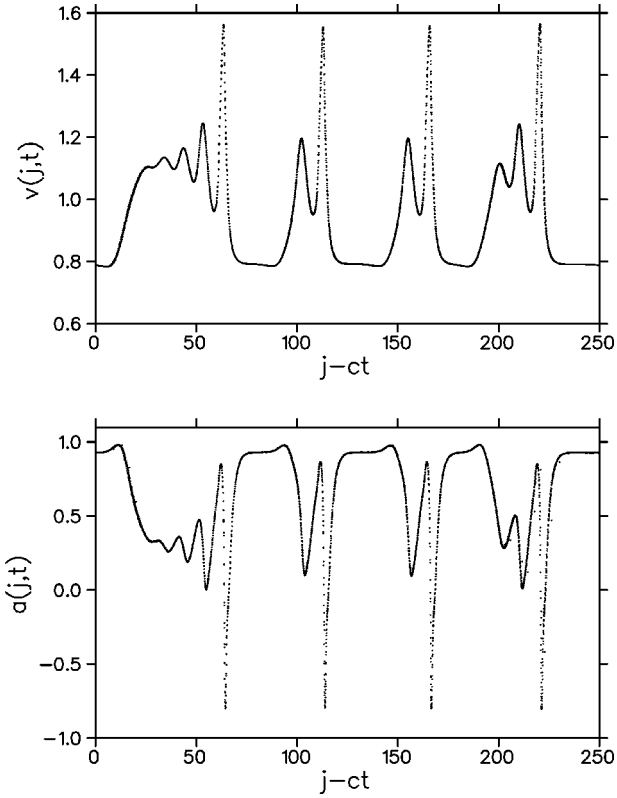

FIG. 9. An example of a multidomain state. The parameters are the same as in Fig. 5.

this method is a very accurate way to measure the front velocity c. The precursors and tails of both fronts are nonoscillating and oscillating, respectively. Furthermore, the oscillatory tail of the front on the left decays roughly two times slower than the precursor of the front on the right. Both observations are in full agreement with our analytical reasoning above.

C. Multidomain states

Starting from an arbitrary initial condition one obtains either a uniform sliding state (if a stable one exists) or a multidomain state, but only rarely a two-domain state. This is especially true for large systems. It is a very general behavior of bistable spatially extended systems, at least for the initial phase of the dynamics. Different parts of the system establish themselves independently into one of the bistable states. It is therefore natural that several domains occur. After the initial formation of a multidomain state, domains may shrink and eventually disappear on a slow time scale. This can be understood by the fact that an attractive force between the fronts exists [29]. This force is caused by the overlap of the precursor, and the tail of the neighboring fronts. It can be calculated by singular perturbation theory [19,29]. In the case of nonoscillating precursors and tails, the force decreases exponentially with distance [29]. In our case, where the tail is oscillating, the resulting force is also oscillating [19,30]. Therefore, equilibrium positions are possible where a pair of two fronts form a bound molecule. The available distances between the fronts are quantized. Figure 9 shows an example where this quantization is clearly seen. In accordance with Shilnikov's theorem, such molecules are possible only if the oscillatory tail decays slower than the nonoscillatory one [31,32] which is indeed the case (see Sec. IV B). As a consequence the system shows spatial chaos.

For values of F near higher order resonances, the velocity-distance characteristic of the uniform sliding state shows several resonance folds. Thus multidomain states are possible which are built up from more than two different domain types. All our numerical experiments have shown that no matter how many domain types occur in the transient, at the end (i.e., in the long-time limit) only two or three domain types survive. Furthermore, all fronts travel with the same velocity c. There is a simple argument why more than three domain types are inconsistent with the last fact. Consider the case of four different domain types with $a_1<a_2<a_3<a_4$ and $v_1>v_2>v_3>v_4$. Between two consecutive values a_i and a_{i+1}, there should be no additional stable state and only one unstable state. Thus if two such domain types are neighbors, the states are functionally related in accordance with Eq. (27). Let us assume a sequence of domains from right (domain type 1) to left (domain type 4). Using Eq. (27), we obtain $a_{i+1}=A(a_i)$. This sequence is therefore uniquely determined by a_1. Now the condition that all fronts have the same speed cannot be fulfilled because there is only one free variable but (at least) two conditions, namely, $c_{12}=c_{23}=c_{34}$. Thus four different domain types are in contradiction with the observation concerning the front velocities.

For $F<b$, domainlike solutions occur where in one domain state the particles sit in potential wells (average particle

distance a is an integer multiple of 2π, e.g., $a=0$) and do not move. Such so-called traffic-jam solutions were already reported by Braun and co-workers [15–17]. They mainly occur near integer values of $a/2\pi$, where the domainlike states discussed in this section are not possible.

V. CONCLUSION

In this paper the regular sliding states (periodic and quasiperiodic solutions) of the FK model are investigated for large chains ($N>100$) and for values of γ, b, and F, where all forces in the equation of motion (1) are of the same order.

Instead of classifying these attractors to be either periodic or quasiperiodic, a more informative distinction is whether their locally average particle density is uniform or not. In a periodic state the density is uniform because all particles perform the same motion, only shifted in time. The motion of the whole chain is completely determined by a single periodic function, the dynamical hull function. The velocity-force characteristics of the periodic attractors show peaks at certain values of the velocity. These peaks are caused by resonances of the ''washboard'' wave. In the frame of the center of mass of the chain, the external potential can be seen as a wave (washboard wave) with wave number a (which is the inverse average particle density) and frequency v (which is the average sliding velocity). Resonances occur for those values of v where n washboard waves are able to decay into a phonon [wave number k, frequency $\omega(k)$] in accordance with ''momentum'' and ''energy'' conservation [i.e., $k=na$ and $\omega(k)=nv$]. A similar process with a decay into two phonons (parametric resonance) explains why the uniform sliding state may be unstable even though the differential mobility is positive.

Quasiperiodic states emerge from instabilities of uniform sliding states. They are characterized by domains of different average particle densities. In each domain the average particle velocity is uniform and *nonzero*. The walls between neighboring domains all move with the same velocity. This domain-wall or front velocity is different from the velocity of the center of mass. Thus each particle goes through all domains. In a quasiperiodic attractor, not more than three different domain types are possible. For chains close to the most commensurate case (i.e., a is an integer multiple of 2π) the average particle velocity is zero in one domain. In this so-called traffic-jam state [15] the particles alternately switch between stationarity and sliding. Because the traffic-jam state exists for also finite temperatures [15,17], states with different sliding domains will presumably survive finite temperatures.

In this paper we have developed a quasicontinuum description of the FK model on the basis of slowly varying locally averaged inverse density a and velocity v. That is, a and v slowly depend on the particle index j and the time t. A set of partial differential equations [Eqs. (31)] governs the dynamics of the variables (assuming j to be a continuous space variable). It is not possible to solve these partial differential equations analytically. But it is quite helpful to understand (i) why the FK model organizes itself into domainlike states with domain states which are not determined from outside, (ii) why there are not more than three different domain types, (iii) why the size of the domains is quantized, (iv) why states with several domains of the same type are possible, (v) why a multidomain state can be seen as an example of spatial chaos, and (vi) why for a fixed value of the external force F the number of stable states increases exponentially with N. The huge number of stable states leads to multihysteretic behavior like in a ferromagnet, where the position in the velocity-force characteristic strongly depends on the history.

The phenomenon of domainlike states, where each domain is characterized by a spatially periodic but stationary solution, has already been found in hydrodynamical pattern formation (Taylor-Couette [33] and Rayleigh-Bénard [34] system). Theoretically this behavior has been modeled by nonlinear phase equations [19,35,36]. In our case the domain states are periodic in space and time; they are traveling waves.

In experiments where locally resolved measurements are not possible, the most important consequence of the domainlike sliding states are (i) quasiperiodicity in the time signals like the velocity of the center of mass, (ii) flattening of the resonance peaks (see Fig. 6), and (iii) multihysteretic behavior. Many of these features should disappear for small values of N if they are caused by domainlike states. Because the inertia term is important for these states, we do not expect it in CDW systems. In adsorbate layers and ionic conductors the appearance of such states should be possible, but it may be difficult to drive them *uniformly* and to measure the velocity-force characteristic. The ideal systems to check our theory are Josephson-junction arrays, because the force and the velocity correspond to the driving current and the voltage, respectively. Furthermore, the damping constant γ and the number of junctions N can be chosen by the fabrication process. The average distance $a=2\pi M/N$ is also easily accessible, because the number M of flux quanta can be chosen by the initial preparation of the system. Thus for rings of more than 50 Josephson junctions we predict the occurrence of domainlike sliding states.

ACKNOWLEDGMENTS

We thank H. Thomas for a critical reading of the manuscript. This work was supported by the Swiss National Science Foundation.

APPENDIX A: NUMERICAL AND ANALYTICAL APPROXIMATIONS OF THE HULL-FUNCTION EQUATION (9)

In this appendix we describe the numerical scheme we have used to solve the differential delay equation (9) for the dynamic hull function $f(\varphi)$. In the simplest case, this scheme also leads to a nonlinear analytical approximation.

Because of Eqs. (8) and (10), we expand the dynamic hull function f into a Fourier series

$$f(\varphi)=\sum_{m=1}^{\infty} f_m e^{im\varphi}+\text{c.c.} \tag{A1}$$

In the numerical approximation we replace this infinite series by a finite one with a cutoff M, i.e., $\Sigma_{m=1}^{\infty}\rightarrow\Sigma_{m=1}^{M}$. Plugging

this ansatz into the differential delay equation (9) leads to a set of nonlinear algebraic equations for the coefficients $\{f_1, f_2, \ldots, f_m, \ldots\}$:

$$[(mv)^2-\omega^2(ma)-i\gamma mv]f_m=bI_m(f_1,f_2,\ldots,f_j,\ldots), \tag{A2}$$

where $\omega(k)$ is the phonon dispersion relation (14), and

$$I_m(f_1,f_2,\ldots,f_j,\ldots)\equiv\frac{1}{2\pi}\int_0^{2\pi}\sin[\varphi+f(\varphi)]e^{-im\varphi}d\varphi. \tag{A3}$$

The driving force F does not appear in the set of equations (A2). That is, we first obtain a solution of Eq. (A2) for a given value of v. After that, we obtain the corresponding value of F by using Eq. (12), i.e.,

$$F=\gamma v\left(1+2\sum_{m=1}^{\infty}m^2|f_m|^2\right). \tag{A4}$$

In the numerical approximation, we solve the set of M algebraic equations (A2) with the Newton method. The most time-consuming part of the computation is the calculation of I_m. In order to speed up the computation we restrict ourselves to values of the cutoff M which are powers of 2. Now we are able to calculate $\{I_1, \ldots, I_M\}$ from $\{f_1, \ldots, f_M\}$ by two fast Fourier transformations (FFT's). The first one is an inverse FFT which calculates the hull function in real space. Next we calculate $\sin[\varphi+f(\varphi)]$. The second FFT yields $\{I_1, \ldots, I_M\}$.

In order to obtain reliable results, the value of the cutoff M has to be chosen carefully. Due to the FFT the hull function is approximated on a lattice with lattice constant π/M. Because of Eq. (7), this corresponds to a time resolution $\Delta t=\pi/(vM)$ of $x_j(t)$. The fastest time scale in the system is given by 2π divided by the maximum phonon frequency, which is 2 in accordance with Eq. (14). Assuming that the fastest time scale has to be resolved at least by two steps Δt, we obtain reliable results only if

$$v\gtrsim\frac{2}{M}. \tag{A5}$$

All results reported in this paper are obtained for $M=32$. Thus v has to be larger than 0.06.

For $M=1$, we obtain an analytic result parametrized by the modulus of f_1. We write

$$f_1=\frac{A}{2}e^{i\psi}. \tag{A6}$$

Due to the integral representation of the Bessel functions of the first kind, we can obtain $I_1(f_1)$. Together with Eq. (A2), we obtain

$$[v^2-w^2(a)]A=b[J_2(A)-J_0(A)]\sin\psi, \tag{A7}$$

$$\gamma vA=b[J_2(A)+J_0(A)]\cos\psi. \tag{A8}$$

The elimination of ψ leads to polynomial of second order in v^2. Thus we obtain an analytic solution parametrized by A:

$$v(A)=\left(\omega^2(a)-\frac{\tilde{\gamma}^2}{2}\pm\sqrt{\frac{\tilde{\gamma}^4}{4}-\omega^2(a)\tilde{\gamma}^2+\left(\frac{\tilde{b}}{A}\right)^2}\right)^{1/2}, \tag{A9a}$$

with

$$\tilde{\gamma}\equiv\frac{J_0(A)-J_2(A)}{J_0(A)+J_2(A)}\gamma \tag{A9b}$$

and

$$\tilde{b}\equiv[J_0(A)-J_2(A)]b. \tag{A9c}$$

Using Eq. (A4), we obtain

$$F(A)=\gamma v(A)\left(1+\frac{A^2}{2}\right). \tag{A9d}$$

APPENDIX B: LINEAR STABILITY ANALYSIS OF THE UNIFORM SLIDING STATE

In this appendix we explain our procedure to calculate numerically the stability of the uniform sliding state. Furthermore, we derive an approximation for v_c.

Plugging the Floquet-Bloch ansatz (19) into the linearized equation of motion (18) leads to

$$\begin{aligned}v^2c_k''(\varphi)+(2\lambda_k+\gamma)vc_k'(\varphi)+(\lambda_k^2+\lambda_k\gamma)c_k(\varphi)\\ =c_k(\varphi-a)e^{-\frac{2\pi i}{N}k}+c_k(\varphi+a)e^{\frac{2\pi i}{N}k}-2c_k(\varphi)\\ -b\,\cos[\varphi+f(\varphi)]c_k(\varphi).\end{aligned} \tag{B1}$$

The Fourier ansatz

$$c_k(\varphi)=\sum_{m=0}^{\infty}c_{k,m}e^{im\varphi}+\text{c.c.} \tag{B2}$$

turns this equation into a set of infinitely many linear equations:

$$\begin{aligned}\left[\omega^2\left(ma+\frac{2\pi k}{N}\right)+(\lambda_k+imv)^2+\gamma(\lambda_k+imv)\right]c_{k,m}\\ =-b\sum_{m'=0}^{\infty}(K_{m-m'}c_{k,m'}+K_{m+m'}c_{k,m'}^*),\end{aligned} \tag{B3}$$

where

$$K_m\equiv\frac{1}{2\pi}\int_0^{2\pi}\cos[\varphi+f(\varphi)]e^{-im\varphi}d\varphi. \tag{B4}$$

Again we have to choose a cutoff M' to solve this set numerically. In order to be consistent with the cutoff $M=32$ of the Fourier expansion of the hull function f we have chosen $M'=15$. Because of Eq. (19), the stability depends on the number N of particles. For large N the eigenvalues λ_k lead to a continuous function $\lambda(2\pi k/N)$. Since we are mainly interested in large systems ($N>50$), we have chosen $N=100$. It is difficult to check numerically whether the uniform sliding state is stable or not because of the Goldstone mode $\lambda_0=0$. Our numerically obtained value of λ_0 fluctu-

ates around zero because of unavoidable errors. Therefore, our instability criterion reads as follows: The uniform sliding state is unstable if at least one eigenvalue is larger than 0.05. This value is considerably larger than the amplitude of the numerical fluctuations of λ_0.

We are able to obtain an analytical approximation of the largest sliding velocity v_c at which parametric resonance is just able to destabilize the uniform sliding state. We do this for zero damping because physical intuition tells us that v_c decreases monotonically with γ. In fact, for $\gamma \ll 1$ and $b = O(\gamma^0)$, the largest sliding velocity is the undamped one minus a correction term of order γ. The approximation makes three assumptions: (i) Parametric resonance at v_c occurs for that value of q which maximizes $v_1^P(q)$. For $0 \leqslant a \leqslant \pi$ this implies $q = \pi$. (ii) All Fourier coefficients of c_k are zero except $c_{k,0}$ and $c_{k,1}$. (iii) The integrals K_m are calculated only in leading order of b, which yields

$$K_m \approx \frac{1}{2\pi}\int_0^{2\pi} \cos(\varphi) e^{-im\varphi} d\varphi = \frac{\delta_{1,m} + \delta_{-1,m}}{2}, \quad \text{(B5)}$$

where $\delta_{n,m}$ is the Kronecker symbol. With $\gamma = 0$ and these assumptions, Eq. (B3) reduces to

$$\begin{pmatrix} \omega_0^2 + \lambda^2 & b/2 \\ b/2 & \omega_0^2 + (\lambda + iv)^2 \end{pmatrix} \begin{pmatrix} c_{k,0} \\ c_{k,1} \end{pmatrix} = \begin{pmatrix} 0 \\ 0 \end{pmatrix}, \quad \text{(B6)}$$

where

$$\omega_0 \equiv \omega(k) = \omega(a+k) = \omega(a/2 \pm \pi) = 2\cos\left(\frac{a}{4}\right). \quad \text{(B7)}$$

A nontrivial solution of Eq. (B6) implies a zero determinant leading to a characteristic polynomial of second order in $(\lambda + iv/2)^2$. Solutions with a nonzero real part of λ occur only if $(\omega_0^2 - v^2/4)^2 < b^2/4$. Therefore we obtain Eq. (21).

[1] J. Frenkel and T. Kontorova, Zh. Éksp. Teor. Fiz. **8**, 1340 (1938); J. Phys. (Moscow) **1**, 137 (1939).

[2] Several years before Frenkel and Kontorova, Dehlinger already introduced this model in the same context. He studied approximately nontrivial stationary solutions. For more details, see U. Dehlinger, Ann. Phys. (Leipzig) **2**, 749 (1929).

[3] S. Aubry, in *Solitons and Condensed Matter Physics*, edited by A. R. Bishop and T. Schneider (Springer, New York, 1978).

[4] W. Uhler and R. Schilling, Phys. Rev. B **37**, 5787 (1988).

[5] L. Pietronero, W. R. Schneider, and S. Strässler, Phys. Rev. B **24**, 2187 (1981).

[6] S. Aubry, J. Phys. (France) **44**, 147 (1983).

[7] F. Vallet, R. Schilling, and S. Aubry, J. Phys. C **21**, 67 (1988).

[8] L. M. Floría and J. J. Mazo, Adv. Phys. **45**, 505 (1996).

[9] S. Watanabe, H. S. J. van der Zant, S. H. Strogatz, and T. P. Orlando, Physica D **97**, 429 (1996).

[10] G. M. McClelland, in *Adhesion and Friction*, edited by M. Grunze and H. J. Kreuzer, Springer Series in Surface Science Vol. 17 (Springer, New York, 1989).

[11] S. N. Coppersmith and D. S. Fisher, Phys. Rev. A **38**, 6338 (1988).

[12] M. Peyrard and M. D. Kruskal, Physica D **14**, 88 (1984).

[13] K. Shinjo and M. Hirano, Surf. Sci. **283**, 473 (1993).

[14] A. V. Ustinov, M. Cirillo, and B. A. Malomed, Phys. Rev. B **47**, 8357 (1993).

[15] O. M. Braun, T. Dauxoisw, M. V. Paliy, and M. Peyrard, Phys. Rev. Lett. **78**, 1295 (1997); Phys. Rev. E **55**, 3598 (1997).

[16] M. Paliy, O. Braun, T. Dauxois, and B. Hu, Phys. Rev. E **56**, 4025 (1997).

[17] O. M. Braun, A. R. Bishop, and J. Röder, Phys. Rev. Lett. **79**, 3692 (1997).

[18] T. Strunz and F. J. Elmer, in *Physics of Sliding Friction*, edited by B. N. J. Persson and E. Tosatti (Kluwer, Dordrecht, 1996).

[19] M. C. Cross and P. C. Hohenberg, Rev. Mod. Phys. **65**, 851 (1993).

[20] A. A. Middleton, Phys. Rev. Lett. **68**, 670 (1992).

[21] S. Aubry and L. de Seze (unpublished).

[22] S. Aubry and L. de Seze, Festkoerperprobleme **XXV**, 59 (1985).

[23] It should be noted that it is mathematically not evident that Eq. (9) has a solution at all [9]. Numerically we always found at least one solution as long as v is larger than the limit dictated by our numerical scheme (see Appendix A).

[24] H. S. J. van der Zant, T. P. Orlando, S. Watanabe, and S. H. Strogatz, Phys. Rev. Lett. **74**, 174 (1995).

[25] M. Weiss and F. J. Elmer, Z. Phys. B **104**, 55 (1997).

[26] The conjecture in Ref. [18] that a_1 and a_2 are highly rational numbers is generally not true.

[27] G. B. Whitham, *Linear and Nonlinear Waves* (Wiley, New York, 1974).

[28] D. Zwillinger, *Handbook of Differential Equations* (Academic, Boston, 1989).

[29] K. Kawasaki and T. Ohta, Physica A **116**, 573 (1982).

[30] C. Elphick, E. Meron, and E. A. Spiegel, Phys. Rev. Lett. **61**, 496 (1988).

[31] A. Arneodo, P. Coullet, and C. Tresser, Commun. Math. Phys. **79**, 573 (1981).

[32] A. Arneodo, P. Coullet, and C. Tresser, J. Stat. Phys. **27**, 171 (1982).

[33] G. W. Baxter and C. D. Andereck, Phys. Rev. Lett. **57**, 3046 (1986).

[34] J. Hegseth, J. Vince, M. Dubois, and P. Bergé, Europhys. Lett. **17**, 413 (1992).

[35] H. Brand and R. Deissler, Phys. Rev. Lett. **63**, 508 (1989).

[36] H. Riecke, Europhys. Lett. **11**, 213 (1990).